Robust Superomniphobic Micro-Hyperbola Structures Formed by Capillary Wrapping of a Photocurable Liquid around Micropillars

Jaekyoung Kim, Yerin Ryu, Chi Hyung Kim, Seong Gil Heo, Kee-Youn Yoo,* and Hyunsik Yoon*

Superomniphobic surfaces inspired by nature have been studied for decades. Recently, the development of liquid-repelling surfaces has moved from the fabrication of artificial structures to real applications that address friction associated with clothes, paper, and skin. To have superoleophobicity, re-entrant structures such as mushrooms or inverse trapezoids have been suggested. However they can be mechanically fragile, especially under shear stress, because the bottom region is narrow. Here, a facile method to obtain new re-entrant structures is proposed, namely, micro-hyperbola structures, by wetting a photocurable viscous liquid around micropillars by capillary force. It is demonstrated that the formation of the hyperbola structures depends on the spacing ratio between micropillars, and the formation mechanism is explained with a simple model. The micro-hyperbola structure demonstrates robust omniphobicity even after rubbing and abrasion tests. The advantage of the wide fabrication range and the robust superoleophobicity of micro-hyperbola structures enable the uses in practical superomniphobic applications that undergo shear forces.

1. Introduction

Bioinspired liquid-repelling surfaces have been studied for versatile purposes, such as self-cleaning surfaces.[1–10] Many researchers have investigated the principle of superhydrophobicity in living structures, such as lotus leaves, rice leaves, and termite wings, and they found that the liquid-repelling properties were due to low surface tension and surface roughness.[1–10] In particular, the air trapping strategy of rough surfaces, as explained by the Cassie model, is the reason for superhydrophobicity, and researchers have designed and fabricated artificial superhydrophobic surfaces following the model.[9,10] In particular, high aspect ratios or hierarchical structures have been exploited to demonstrate superhydrophobicity.[5] However, high-aspect-ratio microscale structures are mechanically weak under shear forces, rubbing, or abrasion. Due to their fragile characteristics, high-aspect-ratio structures are considered to not be suitable for real applications, and finding a solution that possesses mechanical robustness as well as the desired surface properties has become an important issue. Recently, robust superhydrophobic surfaces have been proposed by using two different length scales: nanostructures that repel water, and microscale structures that protect the nanostructures and confer durability.[11–14]

In the case of low-surface-tension liquids, such as oil, high-aspect-ratio structures are not sufficient. Tuteja explained that a re-entrant structure is necessary to cause low-surface-tension liquid droplets to float on a surface because no solid surface has a surface energy that is low enough to produce an oil contact angle higher than 90°.[15] Additionally, researchers have studied the effect of re-entrant structures from living creatures, such as springtails, on omniphobicity.[15–26] To achieve oil repellency, re-entrant structures, such as hoodoo,[15] mushroom,[17] T,[18] inverted trapezoidal structures,[19] and doubly re-entrant shapes[20–26] have been proposed. One of the challenges in realizing artificial superoleophobic surfaces is the complexity of their fabrication. Methods of photolithography with a scattering film[19] and optical fluidization of azopolymers[27] were used to fabricate re-entrant polymeric structures. To realize more complicated re-entrant structures, microfabrication methods[20–26,28] such as photolithography followed by reactive ion etching and two-photon polymerization[25] have been developed. However, techniques such as photolithography and reactive ion etching process require sophisticated equipment. Another problem that limits their practical is mechanical fragility: the suggested re-entrant structures are wide at the top and narrow at the bottom. This configuration means that the structures are not robust under shear forces, such as those imposed by rubbing against clothes or paper. For real applications of superoleophobicity, we need new methods that produce robust structures that are

J. Kim, S. G. Heo, Prof. H. Yoon
Department of New Energy Engineering
Seoul National University of Science & Technology
Seoul 01811, Republic of Korea
E-mail: hsyoon@seoultech.ac.kr

Y. Ryu, Prof. K. Y. Yoo, Prof. H. Yoon
Department of Chemical Engineering
Seoul National University of Science & Technology
Seoul 01811, Republic of Korea
E-mail: kyyoo@seoultech.ac.kr

C. H. Kim, Prof. K. Y. Yoo, Prof. H. Yoon
Department of Chemical and Biomolecular Engineering
Seoul National University of Science & Technology
Seoul 01811, Republic of Korea

The ORCID identification number(s) for the author(s) of this article can be found under https://doi.org/10.1002/adfm.202010053.

resistant to damage even under shear forces and simple and inexpensive fabrication methods that are suitable for widespread use.

Here, we propose a facile method of contacting micropillars on a photocurable liquid layer to form hyperbola structures. The liquid layer coats the sidewalls of the micropillars by capillary wetting. By controlling the SR of a pillar array, we produce separated hyperbola structures, although the top area between pillars is connected under certain conditions. We demonstrate the SR dependence by preparing re-entrant structures and explain the relationship with a model. The hyperbola structures coated by fluorinated layers have superomniphobicity. Furthermore, we fabricate hyperbola structures from low surface tension materials, such as per-flouropolyether (PFPE), by double replica molding, and the resulting structures show robustness under shearing by a Kimwipe and the application of weight on sandpaper.

2. Results and Discussion

2.1. Fabrication of Microsized Hyperbola-Shaped Structure Arrays

Figure 1a shows the fabrication method for the hyperbola-shaped structures by using capillary wrapping of a liquid prepolymer around polyurethane acrylate (PUA) micropillar
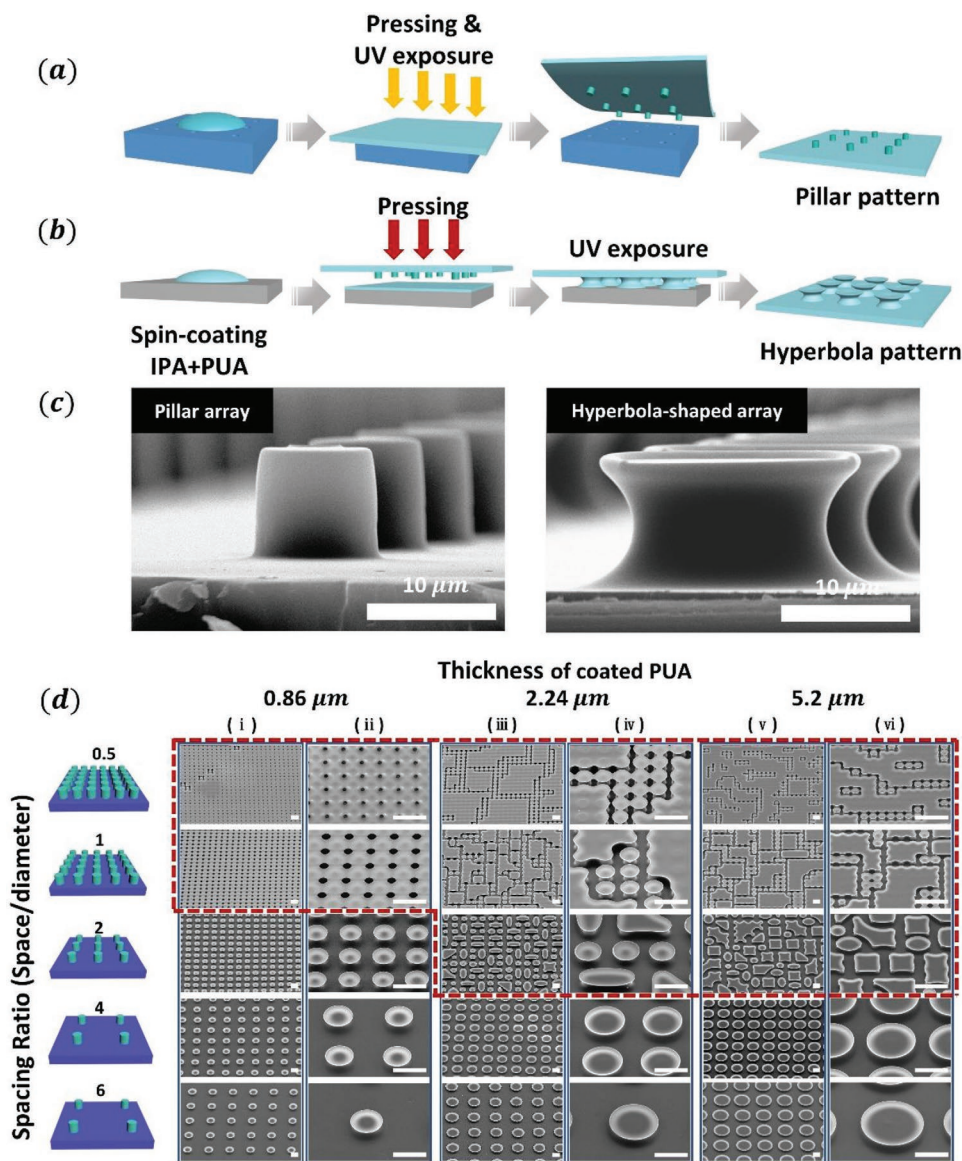
Figure 1. Fabrication schematics of a) the micropillar structure and b) the micro-hyperbola structure. c) Cross-sectional SEM images of the micropillar structure and the micro-hyperbola structure. d) SEM images of the microscale structures fabricated with different SRs (from 0.5 to 6) and thickness of the photocurable liquid PUA coating (from 0.86 to 5.2 μm). i) Micropillar array after liquid prepolymer coating when the coating thickness was 0.86 μm and ii) magnified SEM image of (i). iii) Micropillar array after liquid prepolymer coating when the coating thickness was 2.24 μm and iv) the magnified SEM image of (iii). v) Micropillar array after liquid prepolymer coating when the coating thickness was 5.2 μm and vi) magnified SEM image of (v). The red rectangle represents the range of the fabrication of connected structures (scale bars: 10 μm).

ADVANCED
SCIENCE NEWS
www.advancedsciencenews.com

ADVANCED
FUNCTIONAL
MATERIALS
www.afm-journal.de

arrays. First, we prepared micropillars fabricated by replica molding.[29,30] After dropping a photocurable liquid prepolymer (PUA 311) on a master with hole patterns, we placed a polyethylene terephthalate (PET) film onto the liquid, crosslinked the materials with UV light, and detached the PET film with PUA micropillar patterns from the master (Figure 1a). We prepared a silicon wafer coated with liquid prepolymer (PUA 301). We dropped the liquid mixture onto the silicon wafer and spin-coated the samples. Then, we placed the prepared film with micropillars upside-down onto a silicon wafer coated with liquid prepolymer, pressed the film lightly to achieve contact between the micropillars and liquid-coated wafer, and held them together for 10 min (Figure 1b). During contact without external forces, the liquid PUA prepolymer wetted the sidewall of the micropillars by capillary force, and there is no significant change after 10 min (Figure S1, Supporting Information). After UV exposure to crosslink the liquid prepolymer around micropillars, we detached the film from the silicon wafer, and the hyperbola structures were bonded to the substrate film because of the weak adhesion between the silicon wafer and the crosslinked PUA. To achieve complete crosslinking, we exposed the sample to UV light for 2 h. We note that the PUA (311) used to make the micropillars rigid during pressing onto the silicon wafer and the PUA (301) used to promote capillary action had good compliance and high tensile strength during detachment from the silicon wafer.[29,30] Figure 1c shows a cross-sectional scanning electron microscopy (SEM) image of the micropillars (10 µm in diameter and 10 µm in height) and hyperbola structures formed by using the capillary wetting of liquid PUA (2.24 µm and SR = 2) around the micropillars. The formation of hyperbola structures by the capillary wrapping could be applied to various geometries such as different sizes of pillars, polygonal pillars, or line patterns as shown in Figure S2, Supporting Information.

2.2. Control of the Hyperbola Structure Shape

The geometric shape of the polymeric structures resulting from wetting of the liquid prepolymer around the micropillars can be controlled by the coating thickness of the liquid prepolymer as well as the micropillar SR. We fixed the height (H) and the diameter of the micropillars to 10 µm and conducted experiments with different coating thicknesses and SRs. To control the coating thickness of the prepolymer, we adjusted the viscosity of the liquid prepolymer by changing the mixing ratio with IPA (PUA: IPA) from 1:3 to 1:0.5 and fixed the spinning speed at 3000 rpm. The coating thicknesses corresponding to different mixing ratios were 0.86, 1.24, 2.24, and 5.2 µm. The coating thickness was measured by cross-sectional SEM (Figure S3, Supporting Information) after UV crosslinking. The SR, which is defined by the ratio of the spacing between pillars to the pillar diameter, was designed to vary from 0.5 to 6. SEM images of the experimental results are shown in Figure 1d. When the SR was 2 or less, the top areas were connected to each other, except when the coating thickness was 0.86 µm and SR was 2. When the SR was 4 and higher, we obtained separated structures, and the diameter increased with increasing coating thickness.

Figure 2a illustrates the geometry of the mold with micropillars and the substrate coated with liquid prepolymer (D = diameter of pillars, H = height of pillars, V_{pillar} = volume of a micropillar, V_{space} = volume of the space between micropillars, d = minimum length between pillars, and t = thickness of the coated liquid prepolymer). The prerequisite for the formation of hyperbola structures is that the thickness of the liquid prepolymer, t, should be small enough to not fill the whole volume of the void area. We can obtain the appropriate conditions by achieving mass balance with the assumption of a fixed density, as shown below.

$$(D+d)^2 t < (D+d)^2 H - \left(\frac{D}{2}\right)^2 \pi \tag{1}$$

$$t < \left(1 - \frac{\pi}{4}\left(\frac{1}{1+\frac{d}{D}}\right)^2\right)H \tag{2}$$

For example, when SR is 1, the coating thickness should be lower than 8.04 µm. When the prepolymer does not fill the entire void volume, the prepolymer around the pillars (Figure 2b) can wet the outside of the micropillar sidewalls by capillary action during contact between the micropillars and the silicon wafer coated by the prepolymer. We note that the prepolymer in the center region of the four pillars remained on the substrate, as shown in Figure S4, Supporting Information.
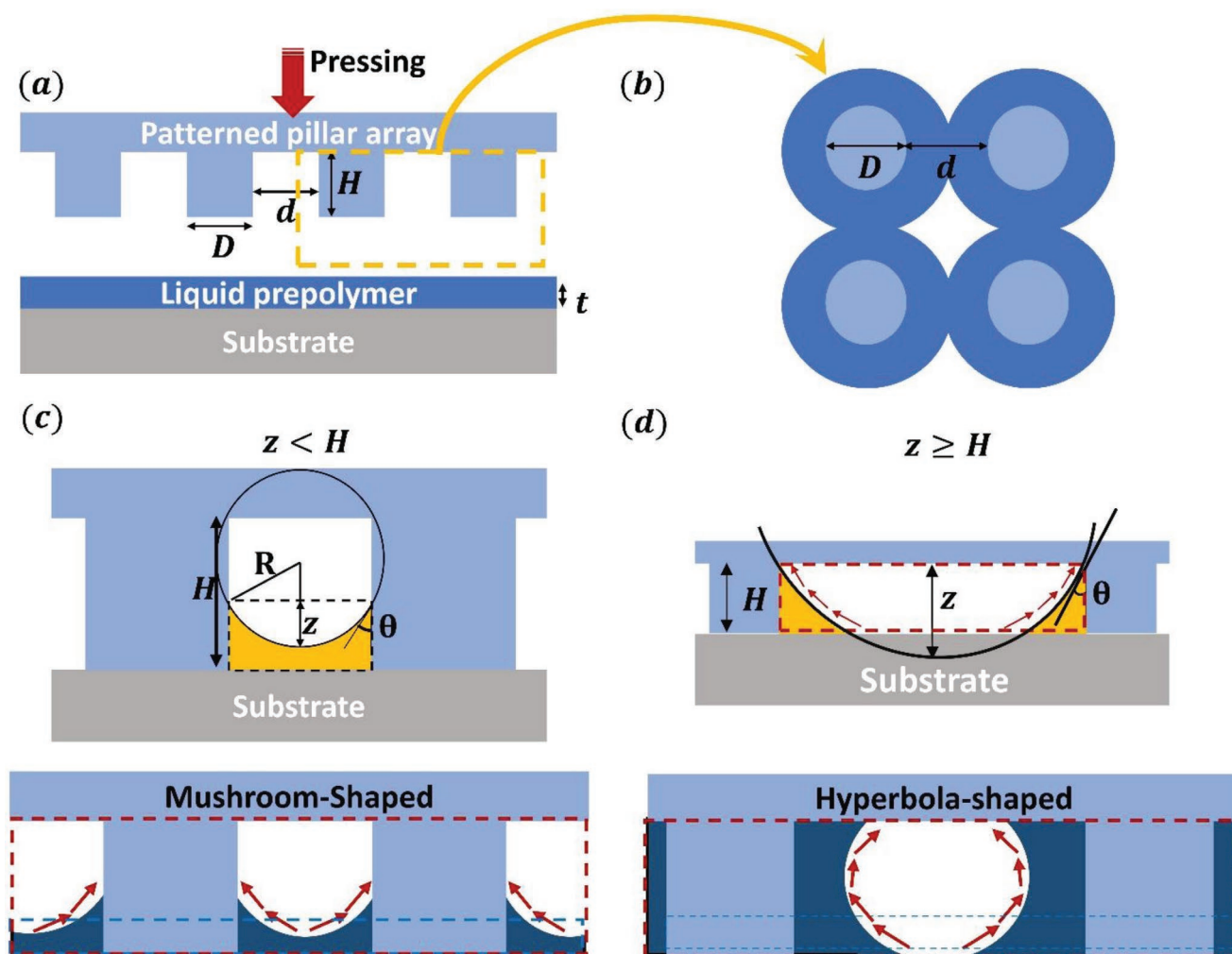
When there was a high aspect ratio, a meniscus formed with an acute contact angle, as shown in Figure 2c. The contact angle θ of the liquid prepolymer on the surface of the micropillars is given by:

$$\cos\theta = \frac{\gamma_{pillar} - \gamma_{prepolymer-pillar}}{\gamma_{prepolymer}} \tag{3}$$

where γ_{pillar} and $\gamma_{prepolymer}$ are the surface energy of the solidified micropillars and liquid prepolymer, respectively; and $\gamma_{prepolymer-pillar}$ is the interfacial energy between the pillars and the prepolymer.[31] Because the interfacial tension was not known, we measured the contact angle with a contact angle meter, and the angle obtained was 22°. From the illustration of the meniscus shown in Figure 2c, we calculated the height of the meniscus (z) between the maximum and minimum points, as shown below:

$$z = \frac{1 - \sin\theta}{2\cos\theta}d \tag{4}$$

where θ is the contact angle and d is the distance between the micropillars.[31] In previous work on residue-free nanoimprint lithography, we reported that there are two cases for the relation between the height of a meniscus resulting from capillary rise (z) and the height of micropillars (H).[31] When z is lower than the pillar height H (**Figure 3**c), the prepolymer connects two pillars, which is not desirable for the fabrication of separated structures. When z is higher than H (Figure 3d), dewetting of the liquid prepolymer occurs on the substrate in the center

ADVANCED
SCIENCE NEWS
www.advancedsciencenews.com

ADVANCED
FUNCTIONAL
MATERIALS
www.afm-journal.de

Figure 2. Schematic illustrations of a micropillar array placed on a liquid prepolymer-coated wafer: a) side view and b) top view. The movement of liquid prepolymer when a micropillar array was placed against a coated wafer in the cases of c) $z < H$ and d) $z > H$.

region between micropillars, and the prepolymer wets from the sidewalls to the roofs of the upside-down pillar arrays. After detaching the sample from the silicon substrate, we obtained separated hyperbola structures. When we used the measured contact angle of 22° in Equation (3), the following conditions for pillar separation were obtained:

$$z = 0.34d > H, d < 29.7\,\mu m \tag{5}$$
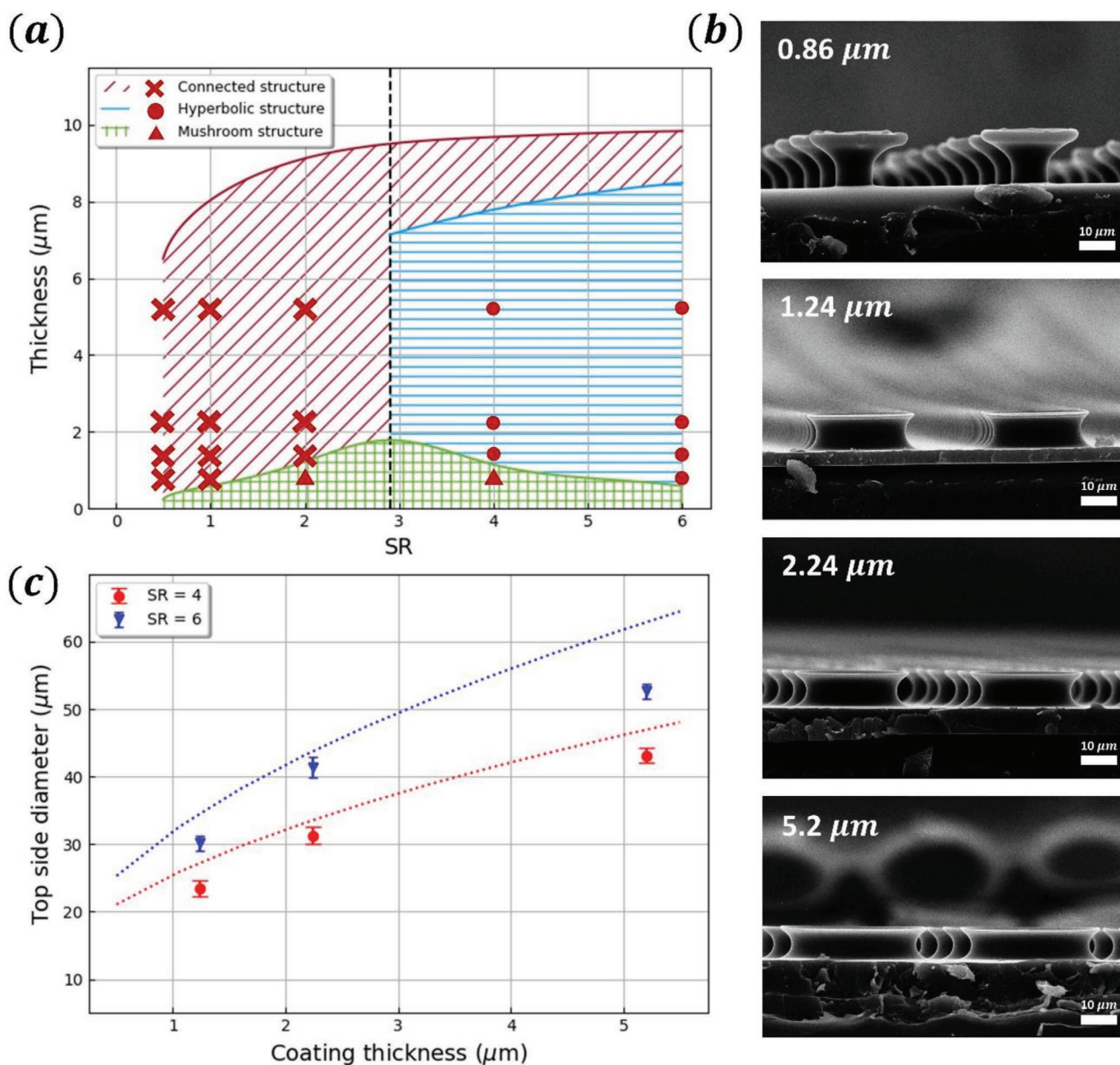
Because the SR is defined as d/D and the diameter of a pillar is fixed to 10 μm, the condition for the formation of separated hyperbola structures by capillary rise is $SR > 2.97$. This result is in good agreement with the experimental results (Figure 1) except for the condition of a thin prepolymer coating thickness ($t = 0.86\,\mu m$).

Even in the case of $z < H$, the capillary bridge can be separated when the prepolymer volume is smaller than the critical thickness; under this condition, the center region of the meniscus touches the substrate surface, as shown in Figure 2c. The critical thickness (t_c) can be calculated from the volume balance, as shown below:

$$\int_0^z \pi x^2 \, dy - \frac{\pi}{4} D^2 z = \frac{\pi}{4} (D+d)^2 t_c \tag{6}$$

where $x = \frac{D+d}{2} - \sqrt{R^2 - (y - R^2)}$ and $R = d/2\cos\theta$. A detailed derivation of the equation can be found in Figure S5, Supporting Information. When we assume that the SR is 2, the calculated critical thickness is 0.96 μm, which means that the pillars can be separated with a mushroom shape when the coating thickness is less than 0.96 μm.

In accordance with Equation (5), the critical thickness was plotted as a function of the SR in Figure 3a. When the coating thickness was less than the critical thickness, we obtained separated mushroom structures. When the coating thickness was higher than the critical thickness, however, the mushroom structures were connected, as shown in Figure 1. Figure 3b shows cross-sectional SEM images of samples with various coating thicknesses and a fixed SR ($SR = 4$). As shown in the top image of Figure 3b, mushroom structures were formed when the coating thickness was 0.86 μm and SR was 4. On the other hand, hyperbola structures were obtained when the coating thickness was higher than the critical thickness, as

**ADVANCED
SCIENCE NEWS**

www.advancedsciencenews.com

**ADVANCED
FUNCTIONAL
MATERIALS**

www.afm-journal.de

Figure 3. a) Diagram showing the creation of different structure types (areas and marked points represent the estimated and actual values, respectively, of the connected structure, the hyperbola structure, and the mushroom structure). b) Profiles of processed structures with increasing coating thickness from 0.86 to 5.2 µm with fixed *SR* (*SR* = 4). c) Graph showing that the diameter increased with increasing coating thickness.

shown in Figure 3b, and the diameter of the hyperbola structures increased with increasing coating thickness. We used the volume balance again to calculate the diameters under various coating thicknesses and SR values. A detailed calculation is shown in the supporting information (Figure S6, Supporting Information). Figure 3c shows the experimental data and the calculated results. The calculated data were slightly less than the experimental results because the calculations corresponded to the ideal case where the liquid wets all the pillars and the liquid density is the same as that of the solid. From the experimental results and the model, we can predict the fabrication range of hyperbola structures and mushroom structures. The

red region in Figure 3a represents the range of interconnected structures, but it is not appropriate to replicate the structures with different materials. The green region represents the range to fabricate mushroom structures. When the SR is smaller than 2.97, mushroom structures can be obtained when the coating thickness is less than the critical thickness, and they are interconnected when the coating thickness is higher. When the SR is higher than 2.97, in contrast, we can obtain hyperbola structures when the coating thickness is higher than the critical thickness and the range is large (blue region in Figure 3a). Additional condition to obtain stable hyperbola structures is that the adhesion of the pillar/prepolymer interface should be

higher than that of the substrate/prepolymer interface after UV crosslinking as below:

$$\left[\pi D_p H + \frac{\pi}{4}\left(D_h^2 - D_p^2\right)\right] W_{p-l} > \frac{\pi}{4}\left(D_h^2 - D_p^2\right) W_{s-l} \tag{7}$$

where D_p and D_h are the diameters of a pillar and a hyperbola, W_{p-l} and W_{s-l} are the works of adhesion at the pillar/liquid prepolymer and substrate/liquid prepolymer interfaces. In this work, the adhesion of the substrate/prepolymer was weak enough to detach the crosslinked polymer from the silicon substrate easily.

2.3. Omniphobicity and Abrasion Test Results of Hyperbola Structures

A hyperbola-shaped structure is also a re-entrant structure because it has a wider area at the top and narrows down to the center. Re-entrant structures have oleophobicity because feature-based vapor pockets are formed between structures. We tested the oleophobicity of the hyperbola structures with nonpolar liquids that have a low surface tension. We prepared micropillar arrays with different SRs to control the shape of the hyperbola structures. In the experiment, we created hyperbola structures with SRs of 4 and 6, which are the required conditions for making hyperbola structures, as shown in Figure 3a. To analyze the wetting properties of the hyperbola structures, we conducted contact angle measurements using 5 µl of n-hexadecane (27 mN m⁻¹ at 20 °C) droplets. To make the surface omniphobic, we treated the surface by using trichloro(1H,1H,2H,2H-perfluorooctyl) silane with a low-vacuum process for 1 h following an UV oxidation treatment to ensure reactivity between the surface and the fluorinated silane. The contact angle was increased by increasing the upper diameter of the hyperbola structures (**Figure 4**a), and the contact angle was higher with an SR of 4 than with an SR of 6. This is because the oleophobicity increases when the spacing between hyperbola structures is small compared to the height of the structures.[16] As shown in Figure 4b, omniphobicity is indicated by the high contact angles for DI water, olive oil, and hexadecane on the transparent film. The solid fraction of the film with hyperbola structure was ≈0.3. Figure 4c shows still images captured from a video of attaching and detaching a hexadecane droplet on the surface of hyperbola-shaped structures several times to prove liquid repellency. The roll-off angle was ≈22°, and a hexadecane droplet escaped from hyperbola structures of a tilted film when we drop the liquid on the surface (See Movie S1, Supporting Information). We note that the surface treatment with fluorinated silane was necessary to have oleophobicity in the hyperbola structure although doubly reentrant structures have been developed to show oleophobicity
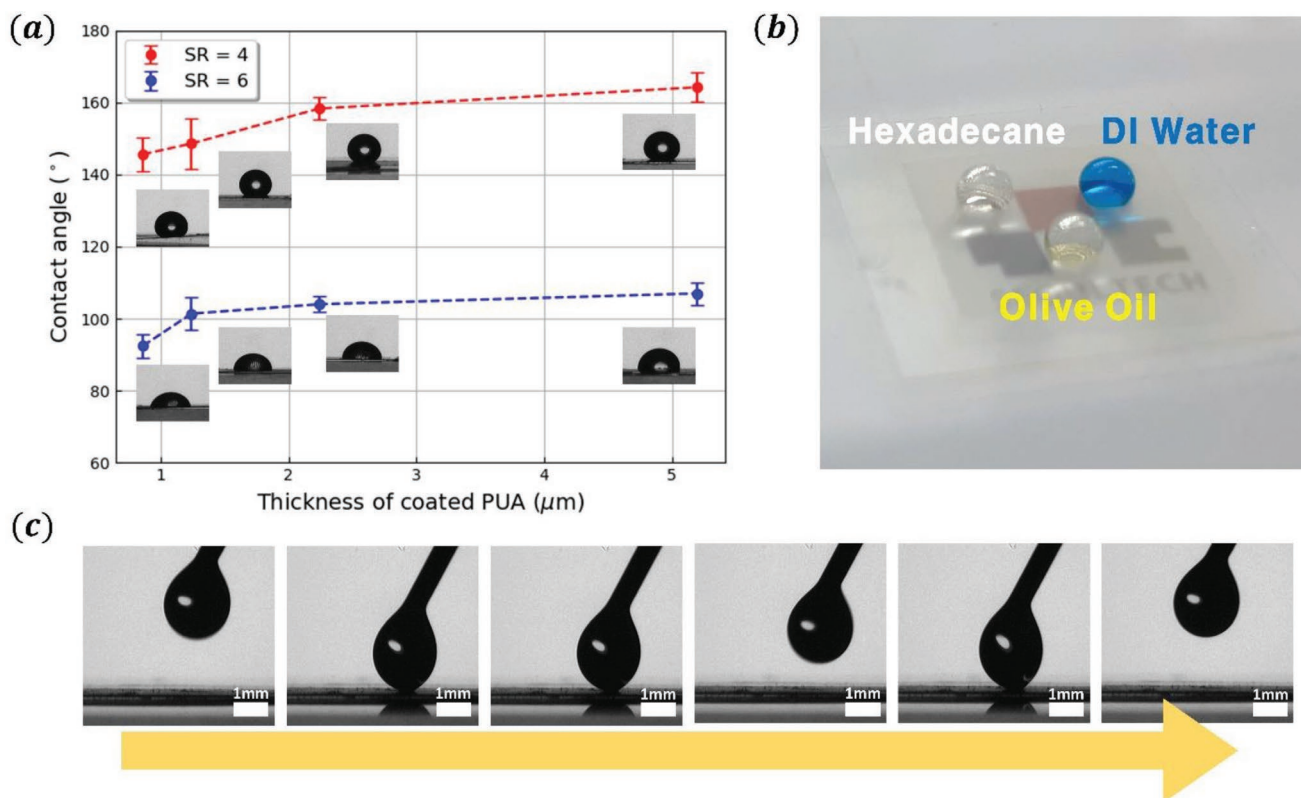
Figure 4. a) Graph showing the contact angle of hexadecane with increasing thickness of the liquid prepolymer coating at different SR values (4 and 6) and photographs of droplets on the surfaces. b) Photograph of DI water, olive oil, and hexadecane droplets on a surface with hyperbola-shaped structures, which was fabricated with a SR = 4 and liquid prepolymer with a thickness of 5.2 µm. c) Photographs of a hexadecane droplet contacting the surface comprising micro-hyperbola arrays.
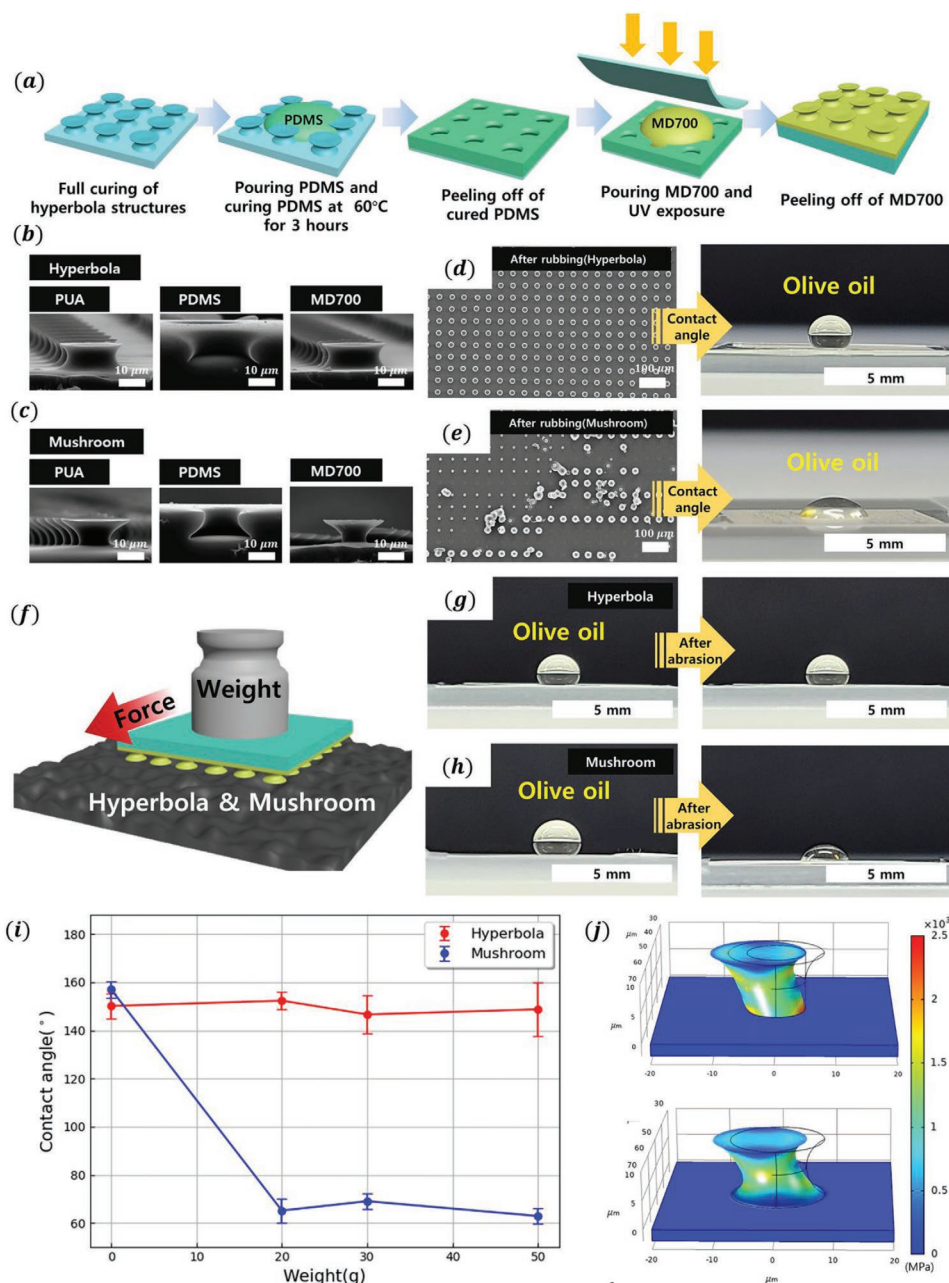
Figure 5. a) Schematics showing the method of replicating samples consisting of PFPE. Cross-sectional SEM images of the PUA mold, PDMS hole patterned mold, and PFPE mold for b) hyperbola structures and c) mushroom structures. SEM image and contact angle image after rubbing test on d) hyperbola structures, and e) mushroom structures. f) Schematic showing the abrasion test method. Photographs showing olive oil contact angle images before and after the abrasion test at 50 g for g) hyperbola structures and h) mushroom structures. i) Graph of surface contact angles with increasing weight on the hyperbola and mushroom structures. j) FEM simulation results showing the stress distribution on a pillar and a hyperbola structure during applying shear stress on upper surfaces.

without the coating of fluorinated species.[21–22] In the reversely tapered re-entrant structures such as hyperbola structures, the contact angle of a liquid droplet should be higher than the taper angle as shown in Figure S7, Supporting Information.[10] As shown in Figure S8, Supporting Information, the contact angle of hexadecane on a PUA is 29°, which is much less than the average taper angle of hyperbola structures (56°). On the other hand, the contact angle of hexadecane on the fluorinated PUA surface is 68°, which satisfied the condition to show oleophobicity. When we use an olive oil droplet, the PUA hyperbola structures show superoleophobicity ($\approx$150°) without surface treatment because the contact angle on a flat PUA is 71°, which is higher than the taper angle. In addition, to keep air pockets in the re-entrant structures, lateral imbibition should be prohibited. Mishra group proposed a method to prohibit the lateral imbibition even in a liquid bath when doubly

**ADVANCED
SCIENCE NEWS**
www.advancedsciencenews.com

**ADVANCED
FUNCTIONAL
MATERIALS**
www.afm-journal.de

reentrant line and cavity structures were used.[22,24–26] Although the isolated hyperbola structures in this work have a limitation to inhibit the lateral imbibition, we expect that line and cavity designs can keep air pockets more stable.

To eliminate the additional treatment with fluorinated silane and maintain a low surface energy, we produced hyperbola structures of PFPE, which has low surface energy due to the fluorine groups in it, by using the double replica molding method (**Figure 5**a).[32] After the preparation of hyperbola structures with PUA, we used polydimethylsiloxane (PDMS) to form inverted hyperbola structures. We have indicated that PDMS was used to replicate re-entrant structures as the stress of PDMS during pulling out of the re-entrant structures is small enough due to their elastic nature.[33] To reduce the stress, we used a PDMS with a 20:1 ratio (prepolymer/crosslinker) to obtain a smaller Young's modulus in this work. Then, we used PFPE to replicate hyperbola structures from the inverted structures, as shown in Figure 5b. To compare the robustness of the hyperbola structures, we fabricated mushroom structures with PFPE with the same method as that used to prepare the PFPE hyperbola structures (Figure 5c). The solid fraction of hyperbola structures is 0.19 and that of the mushroom structures is 0.20. To show the robustness of the hyperbola structures, we rubbed them with a Kimwipe and performed an abrasion test by applying weight on sandpaper.[13] We manually rubbed the hyperbola array consisting of PFPE with Kimwipes (pressing pressure: 4 N cm^{-2}) and the hyperbola structure exhibited better mechanical robustness than the mushroom structure (Figure 5d,e). Figure 5d,e shows SEM images of the rubbed hyperbola and mushroom surfaces. In the rubbed sample consisting of hyperbola structures, the hyperbola structures on the surface maintained their shape and oleophobic properties (Figure 5d). In the case of the sample with a mushroom structure, however, the mushroom structures on the surface were easily disrupted, and the surface lost its oleophobic properties (Figure 5e). In addition, we conducted an abrasion test using standard 400-grit sandpaper to accurately show the robustness of the hyperbola structure surface (Figure 5f). Samples of hyperbola and mushroom structures made of PFPE were placed on top of the sandpaper (facing the rough surface). Then, we put a weight from 20 to 50 g on each sample, and we moved the sample 10 cm to apply shear force (Figure S9, Supporting Information). After applying shear force, we confirmed the wetting properties by using contact angle tests with olive oil (Figure 5g,h). As a result, it was confirmed that the surface of the sample with mushroom-shaped structures lost its oleophobic properties because the contact angle decreased dramatically after the abrasion test. However, in the case of the hyperbola structure, the structure remained stable and retained its oleophobic properties even after the abrasion test until we added a weight of 50 g to the sample (Figure 5i), and the sample maintained a high contact angle. We note that the hyperbola structures lost the oleophobicity when the weight of the abrasion test is 100 g because they were broken as shown in Figure S10, Supporting Information. To compare the robustness of the hyperbola structures to the mushroom structures, we performed a finite element method (FEM) simulation. We designed them with the same pillar diameter (10 μm), height (10 μm), and upper diameter (18 μm). In the hyperbola

structures, the diameter of the central region is 10 μm as shown in Figure S11, Supporting Information. When we applied shear force on the upper surface of the mushroom and the hyperbola structures, the maximum stress of the mushroom is in the baseline and much higher than that of hyperbola structures in the central region (Figure 5j). Figure S10, Supporting Information, shows the breaking point of the mushroom and hyperbola structures and it is in agreement with the prediction from the simulation.

3. Conclusion

We demonstrated a facile method to fabricate omniphobic and robust micro-hyperbola structures by capillary wetting of liquid prepolymers around micropillar structures. Various micro-hyperbola structures were obtained according to the spacing between structures and the thickness of the photocurable material to be coated. From the mass balance model, we proposed criteria that could be used to determine the conditions that would create mushroom structures and hyperbola structures, and the latter showed a wider process range. We tested droplets of water, olive oil, and hexadecane to show omniphobic behavior. The robust micro-hyperbola structures showed superoleophobicity, and we proved their mechanical robustness by rubbing and abrasion tests. This simple fabrication method for the formation of hyperbola structures and the durability of the resulting structures supports the use these materials in practical superomniphobic applications that undergo shear forces.

4. Experimental Section

Materials: The UV-curable prepolymer PUA (PUA 301 & 311) was purchased from Material Chemicals Network Co., Ltd. The PFPE (MD700) was purchased from JUNSUNG Polymer Co., Ltd. Trichloro(1H,1H,2H,2H-perfluorooctyl)silane and IPA were purchased from Sigma-Aldrich and used without further treatment. The silicon wafers were purchased from iCell Co., Ltd. The PDMS was purchased from Dow Corning.

Preparation of the Micropillar Structure Array Sample Consisting of PUA: Patterned silicon masters were fabricated by photolithography followed by a dry etching process. The master had micropillar arrays (10 μm in height and 10 μm in diameter) with different SRs from 1:0.5 to 1:6 over an area of 10 mm × 10 mm. To fabricate replicated hole arrays with PDMS, the PDMS prepolymer was poured onto the patterned silicon masters after mixing the prepolymer and curing agent in a 10:1 weight ratio and curing at 60 °C for more than 4 h. After thermal crosslinking, the cured PDMS replica mold with hole arrays was peeled off from the silicon master. From the PDMS replica mold with hole arrays, PUA micropillar arrays were fabricated by using the replica molding method. The UV-curable PUA liquid prepolymer was dropped onto the PDMS replica mold and covered it with a PET film to spread the prepolymer between the PDMS mold and the PET substrate. Then, the sample was exposed to UV light (450 mJ) for a few seconds to crosslink the PUA prepolymer. When the PET film was detached from the PDMS mold, the PUA micropillars were bonded to the PET film because of the weak adhesion between the PDMS and solidified PUA.

Double Replication to Fabricate PFPE Hyperbola Structures: A PDMS mold fabricated from the original hyperbola structure made with PUA was used to replicate a hyperbola structure composed of PFPE, which is a photocurable and fluorinated material. First, the PDMS prepolymer was poured onto the hyperbola arrays, which were made of PUA,

followed by 3 h of thermal curing at 60 °C. The cured PDMS was peeled off from the hyperbola array. Then, PFPE was poured onto the PDMS mold with the array of hyperbola holes and exposed the sample to UV light. Following this, a PFPE mold consisting of a hyperbola structure was demolded from the PDMS mold.

SEM Characterization: SEM images were taken by using an EM-30 SEM (COXEM; Republic of Korea) with an acceleration voltage of 10 kV. The contact angle images were acquired by a CAM-200 contact angle meter (KSV, Finland). A Fusion Cure 360 (MINUTA Tech, Republic of Korea) UV curing and patterning device (5.0 mW cm^{-2}) was used to cure the photocurable materials.

Contact Angle Measurements: The contact angles were measured by a contact angle meter (CAM 200, KSV Instrument Ltd., Finland). The contact angle images were taken by fitting an outline to the hexadecane droplet circle.

FEM Simulation: The conventional FEM software (COMSOL Multiphysics v. 5.5, structural mechanics module, physics-controlled mesh (basic auto mesh)) was used to obtain the stress distribution on structures fixed on a substrate (fixed constraint mode). Shearing force (0.05 N) was applied using a rigid connector.

Supporting Information

Supporting Information is available from the Wiley Online Library or from the author.

Conflict of Interest

The authors declare no conflict of interest.

Data Availability Statement

Research data are not shared.

[1] F. Xia, L. Jiang, *Adv. Mater.* **2008**, *20*, 2842.
[2] X. Deng, L. Mammen, H.-J. Butt, D. Vollmer, *Science* **2012**, *335*, 67.
[3] X. Deng, L. Mammen, Y. Zhao, P. Lellig, K. Mullen, C. Li, H.-J. Butt, D. Vollmer, *Adv. Mater.* **2011**, *23*, 2962.
[4] G. S. Watson, B. W. Cribb, J. A. Watson, *ACS Nano* **2010**, *4*, 129.
[5] H. Teisala, H. J. Butt, *Langmuir* **2019**, *35*, 10689.
[6] Y. Rahmawan, L. Xu, S. Yang, *J. Mater. Chem. A* **2013**, *1*, 2955.
[7] K. Golovin, D. H. Lee, J. M. Mabry, A. Tuteja, *Angew. Chem., Int. Ed.* **2013**, *52*, 13007.
[8] A. K. Kota, G. Kwon, A. Tuteja, *NPG Asia Mater* **2014**, *6*, e109.
[9] D. Quéré, *Annu. Rev. Mater. Res.* **2008**, *38*, 71.
[10] A. Tuteja, W. Choi, G. H. McKinley, R. E. Cohen, M. F. Rubner, *MRS Bull.* **2008**, *33*, 752.
[11] X. Tian, T. Verho, R. H. A. Ras, *Science* **2016**, *352*, 142.
[12] D. Wang, Q. Sun, M. J. Hokkanen, C. Zhang, F. Y. Lin, Q. Liu, S. P. Zhu, T. Zhou, Q. Chang, B. He, Q. Zhou, L. Chen, Z. Wang, R. H. A. Ras, X. Deng, *Nature* **2020**, *582*, 55.
[13] Y. Lu, S. Sathasivam, J. Song, C. R. Crick, C. J. Carmalt, I. P. Parkin, *Science* **2015**, *347*, 1132.
[14] T. Verho, C. Bower, P. Andrew, S. Fanssila, O. Ikkala, R. H. A. Ras, *Adv. Mater.* **2011**, *23*, 673.
[15] A. Tuteja, W. Choi, M. Ma, J. M. Mabry, S. A. Mazella, G. C. Rutledge, G. H. McKinley, R. E. Cohen, *Science* **2007**, *318*, 1618.
[16] L. Chen, Z. Guo, W. Liu, *J. Mater. Chem. A* **2017**, *5*, 14480.
[17] S. Y. Lee, Y. Rahmawan, S. Yang, *ACS Appl. Mater. Interfaces* **2015**, *7*, 24197.
[18] J. H. Kim, T. S. Shim, S.-H. Kim, *Adv. Mater.* **2016**, *28*, 291.
[19] M. Im, H. Im, J.-H. Lee, J.-B. Yoon, Y.-K. Choi, *Soft Matter* **2010**, *6*, 1401.
[20] G.-T. Yun, W.-B. Jung, M. S. Oh, G. M. Jang, J. Baek, N. I. Kim, S. G. Im, H.-T. Jung, *Sci. Adv.* **2018**, *4*, eaat4978.
[21] T. Liu, C. J. Kim, *Science* **2014**, *346*, 1096.
[22] E. M. Dominguez, S. Arunachalam, J. Nauruzbayeva, H. Mishra, *Nat. Commun.* **2018**, *9*, 3606.
[23] E. M. Dominguez, S. Arunachalam, H. Mishra, *ACS Appl. Mater. Interfaces* **2017**, *9*, 21532.
[24] S. R. Gonzalez-Avila, D. M. Nguyen, S. Arunachalam, E. M. Dominguez, H. Mishra, C.-D. Ohll, *Sci. Adv.* **2020**, *6*, eaax6192.
[25] S. Arunachalam, R. Das, J. Nauruzbayeva, E. M. Dominguez, H. Mishra, *J. Colloid Interface Sci.* **2019**, *534*, 156.
[26] R. Das, Z. Ahmad, J. Nauruzbayeva, H. Mishra, *Sci. Rep.* **2020**, *10*, 7934.
[27] S. M. Kang, J. S. Choi, *Small* **2020**, *16*, 1904612.
[28] J. Choi, W. Jo, S. Y. Lee, Y. S. Jung, S.-H. Kim, H.-T. Kim, *ACS Nano* **2017**, *11*, 7821.
[29] S.-J. Choi, H. N. Kim, W. G. Bae, K.-Y. Suh, *J. Mater. Chem.* **2011**, *21*, 14325.
[30] S. J. Choi, P. J. Yoo, S. J. Baek, T. W. Kim, H. H. Lee, *J. Am. Chem. Soc.* **2004**, *126*, 7744.
[31] H. Yoon, S. H. Lee, S. H. Sung, K. Y. Suh, K. Char, *Langmuir* **2011**, *27*, 7944.
[32] T. Kim, H. Yoon, H.-J. Song, N. Haberkorn, Y. Cho, S. H. Sung, C. H. Lee, K. Char, P. Theato, *Macromol. Rapid Commun.* **2012**, *33*, 2035.
[33] J. Rhee, J. Park, S. Kwon, H. Yoon, H. H. Lee, *Adv. Mater.* **2003**, *15*, 1075.